Dissected arteries were opened longitudinally, and exposed on a phosphor imaging plate (Fuji Imaging Plate BAS-UR, Fuji Photo Film, Japan) for 19 hr. Autoradiographic images were obtained and analyzed by a computerized imaging analysis system (Fuji bio-imaging analyzer FLA 3000). Furthermore, aortic tissues were stained with Oil Red O for plaque area determination. Five regions of interest (ROIs) were placed on the plaque area (target) and the non-plaque area (non-target) in the aortic tissue, as well as three ROIs for background area around each aorta in ARG images. Signal intensities were shown as photostimulated luminescence per unit area (PSL/mm^2), and average values for each are were used for the analysis. The target-to-nontarget ratios (TNRs) were calculated as follows;

TNR = ([Target signal] – [Background signal]) / ([Non-target signal] – [Background signal])

SPECT/CT imaging with WHHL rabbits

WHHL rabbits (17 mo, 3.3-3.5 kg) or control rabbits (NZW rabbit, 17 mo, 3.4 kg) were used for SPECT imaging studies. Rabbits were anesthetized with a bolus injection of sodium pentobarbital (30 mg/kg, i.v.) followed by continuous injection with propofol (10 mg/kg/hr, i.v.). [^{111}In]PS100 or [^{111}In]PS200 (74 MBq) was injected into a marginal ear vein, and SPECT scanning was carried out 48 hr post-injection of liposomes by use of an FX system PET/SPECT/CT scanner (64 frames, 60 sec/frame, Gamma-Medica Inc., USA) using high-resolution parallel hole collimators. After the SPECT study, a CT angiogram was acquired using iohexol as a contrast agent.

After the last scan, rabbits were sacrificed with an overdose of sodium pentobarbital. The aorta was removed and 10 and 5 μm-thick consecutive sections were prepared. The autoradiogram was obtained with a phosphor imaging system (FLA-3000, Fujifilm Corp., Tokyo, Japan) with 10 μm-thick sections. Other 5 μm-thick sections were subjected to immunohistochemical staining for macrophages, Azan-Mallory staining, and Oil-Red O staining. Immunohistochemistry was performed according to the method reported by Tsukada et al. using the rabbit macrophage-specific monoclonal antibody RAM-11 (Dako Corp., Santa Barbara, CA, USA) (*23*), and slices were co-stained with hematoxylin for identification of the nucleus.

Statistical analysis

Data are presented as the mean ± SD. Statistical analysis was carried out using the Mann-Whitney *U*-test or paired *t*-test for comparisons between or within groups, respectively. Statistical significance was established at $P<0.05$.

RESULTS

In vitro uptake of ^{111}In-liposomes to macrophages

The *in vitro* uptake of ^{111}In-labelled liposomes and [^{111}In]$InCl_3$ by mouse peritoneal macrophages are summarized in Fig. 1. Uptake of both sizes was significantly higher for PS liposomes than for PC liposomes. [^{111}In]PS100 showed significantly higher uptake than [^{111}In]PS200. D-serine liposomes accumulated in macrophages, but the level was lower than for L-serine liposomes of each size. Only a slight uptake of [^{111}In]$InCl_3$ was observed.

Biodistribution studies in normal mice

Data are summarized in Tables 1, 2, 3, and 4. High liver uptake was observed for all liposomes investigated. Uptake into spleen was higher for PC liposomes than PS liposomes. Blood clearance was faster for PS liposomes than PC liposomes, and [^{111}In]PC100 showed the slowest clearance.

Ex vivo ARG in apoE-/- mice

En face *ex vivo* ARG showed accumulation of all investigated ^{111}In-liposomes in the plaque area in mice (Fig. 2 A, B, C). Radioactive regions were well matched with Oil Red O staining. The uptake to nonspecific regions was higher in PC liposomes, and the TNRs were lower in PC liposomes than PS liposomes (Fig. 2 D).

SPECT imaging, ex vivo ARG, and histological analysis in WHHL rabbits

Figure 3 summarizes the SPECT, ARG, and histological images in WHHL and normal rabbits. The white arrows indicate the position of the aorta. The atherosclerotic regions were successfully visualized with [^{111}In]PS200 and [^{111}In]PS100, and the clearest image was obtained with [^{111}In]PS200. No aortic accumulation was seen in normal rabbits with [^{111}In]PS200. ARG images of the aortic section showed accumulation of radioactivity in the plaque area in WHHL rabbits. High accumulation of radioactivity was observed in macrophage foam cell area, and radioactivity was low in fibrotic area as shown by Azan-Mallory staining.

DISCUSSION

Macrophage infiltration plays a pivotal role in plaque rupture by releasing inflammatory cytokines and proteases; therefor it is reasonable to target macrophages for vulnerable plaque imaging. Also, it is well known that macrophages are predisposed to phagocytize particles such as liposomes (*13*,*14*). Therefore, in this study, we employed liposomes as carriers for the atherosclerotic region and designed a SPECT imaging probe. In fact, cultured macrophages took up control PC-liposomes, to a certain extent (Fig. 1). Uptake was higher in 100 nm than 200 nm liposomes. In addition, when the "eat-me" signal, PS, was incorporated into the liposome, uptake into cultured macrophages was significantly elevated; furthermore, 'D-isoform PS' showed lower uptake into macrophages than the naturally occurring 'L-isoform PS' (Fig. 1). These results suggest that macrophage targeting succeeded using liposomes, and that target specificity was enhanced by PS modification. D-PS liposomes showed higher accumulation into macrophages than PC liposomes for each size. The negative charge on the surface of the liposome may enhance particle capture by macrophages. We previously reported that [^{18}F]FDG uptake into cultured mouse peritoneal macrophages was 48.8% dose/mg protein with 3 hr incubation (*24*). In this study, the uptake of [^{111}In]PS100 (60.5% dose/mg protein) was greater than that of [^{18}F]FDG. These results show the potential of [^{111}In]PS100 for *in vivo* atherosclerotic plaque imaging.

In the *in vivo* investigation, the atherosclerotic regions were successfully visualized with ^{111}In-labeled PS liposomes in apoE -/- mice. In contrast to *in vitro* results, accumulation was higher in [^{111}In]PS200 than [^{111}In]PS100. Atherosclerotic lesions were visualized by ^{111}In-labeled PC liposomes of both sizes, but nonspecific accumulation was higher with PC liposomes than PS liposomes; thus TNRs were higher in PS liposomes than PC liposomes. The highest TNR was obtained with [^{111}In]PS200 in *in vivo* evaluation. Also, a successful SPECT image was provided by [^{111}In]PS200 in WHHL rabbits. Thus, [^{111}In]PS200 showed the best features for *in vivo* imaging, although [^{111}In]PS100 provided the best results in *in vitro* investigations. In the biodistribution study in normal mice, [^{111}In]PS200 showed somewhat slower blood clearance than [^{111}In]PS100. This may cause the higher accumulation in the atherosclerotic region in [^{111}In]PS200 than [^{111}In]PS100. Also, we observed a slower blood clearance of PC liposomes than PS liposomes. These results suggest that slow blood clearance should accelerate liposome accumulation into the plaque. However, in atherosclerosis imaging, signals from the blood pool disturb the visualization of plaque in the vessel wall; thus, blood clearance of the imaging probe should ideally be not too slow. In general, PEGylation of particles prolongs the blood clearance due to the avoidance from the reticuloendothelial system (RES) (*25*). On the other hand, liver accumulation is seen as liposome uptake into the Kupffer cells, which have similar characteristics as macrophages concerning phagocytosis. However, excessive liver uptake makes it difficult to visualize the small atherosclerotic region in coronary arteries. Therefore, for atherosclerosis imaging, a certain level of PEGylation of liposomes is desirable, which prolongs blood clearance to a limited extent, and which does not disturb phagocytosis by macrophages. Further investigation of liposome PEGylation would be required, to determine the optimal "balance" between macrophage targeting ability and blood clearance.

CONCLUSION

In this study, the atherosclerotic region was detectable by macrophage targeting with radiolabeled liposomes (PS-liposomes), although additional investigations would be needed to improve the *in vivo* biodistribution and plaque accumulation level. Liposomes can act as a platform for various other imaging modalities, such as MRI and optical imaging. Recently, several liposome-based atherosclerosis-imaging probes for various imaging modalities have been reported (*26-28*). Since liposomes are biocompatible and have long histories as drug carriers for human use (*29*), such imaging probes including the liposome system we have described, should be good candidates for clinical use in the future.

ACKNOWLEDGEMENTS

This work was supported by Grants-in-Aid for Scientific Research from Japan Science and Technology Agency (JST), Japan Society for the Promotion of Science (JSPS), Japanese Ministry of Health, Labour and Welfare.

REFERENCES

1. Libby P. What have we learned about the biology of atherosclerosis? The role of inflammation. *Am J Cardiol.* 2001;88(7B):3J-6J.
2. Libby P. Inflammation in atherosclerosis. *Nature.* 2002;420(6917):868-874.
3. Zhang Z, Machac J, Helft G, et al. Non-invasive imaging of atherosclerotic plaque macrophage in a rabbit model with F-18 FDG PET: a histopathological correlation. *BMC Nucl Med.* 2006;6:3.
4. Ogawa M, Ishino S, Mukai T, et al. (18)F-FDG accumulation in atherosclerotic plaques: immunohistochemical and PET imaging study. *J Nucl Med.* 2004;45(7):1245-1250.
5. Rudd JH, Warburton EA, Fryer TD, et al. Imaging atherosclerotic plaque inflammation with [18F]-fluorodeoxyglucose positron emission tomography. *Circulation.* 2002;105(23):2708-2711.
6. Fifer KM, Qadir S, Subramanian S, et al. Positron emission tomography measurement of periodontal (18)f-fluorodeoxyglucose uptake is associated with histologically determined carotid plaque inflammation. *J Am Coll Cardiol.* 2011;57(8):971-976.
7. Tawakol A, Migrino RQ, Bashian GG, et al. In vivo 18F-fluorodeoxyglucose positron emission tomography imaging provides a noninvasive measure of carotid plaque inflammation in patients. *J Am Coll Cardiol.* 2006;48(9):1818-1824.
8. Rudd JH, Myers KS, Bansilal S, et al. Atherosclerosis inflammation imaging with 18F-FDG PET: carotid, iliac, and femoral uptake reproducibility, quantification methods, and recommendations. *J Nucl Med.* 2008;49(6):871-878.
9. Rudd JH, Myers KS, Bansilal S, et al. Relationships among regional arterial inflammation, calcification, risk factors, and biomarkers: a prospective fluorodeoxyglucose positron-emission tomography/computed tomography imaging study. *Circ Cardiovasc Imaging.* 2009;2(2):107-115.

10. Chen W, Bural GG, Torigian DA, Rader DJ, Alavi A. Emerging role of FDG-PET/CT in assessing atherosclerosis in large arteries. *Eur J Nucl Med Mol Imaging.* 2009;36(1):144-151.
11. Deichen JT, Prante O, Gack M, Schmiedehausen K, Kuwert T. Uptake of [18F]fluorodeoxyglucose in human monocyte-macrophages in vitro. *Eur J Nucl Med Mol Imaging.* 2003;30(2):267-273.
12. Bucerius J, Mani V, Moncrieff C, et al. Impact of noninsulin-dependent type 2 diabetes on carotid wall 18F-fluorodeoxyglucose positron emission tomography uptake. *J Am Coll Cardiol.* 2012;59(23):2080-2088.
13. Stossel TP. Phagocytosis (first of three parts). *N Engl J Med.* 1974;290(13):717-723.
14. Pratten MK, Lloyd JB. Pinocytosis and phagocytosis: the effect of size of a particulate substrate on its mode of capture by rat peritoneal macrophages cultured in vitro. *Biochim Biophys Acta.* 1986;881(3):307-313.
15. Fadok VA, Voelker DR, Campbell PA, Cohen JJ, Bratton DL, Henson PM. Exposure of phosphatidylserine on the surface of apoptotic lymphocytes triggers specific recognition and removal by macrophages. *J Immunol.* 1992;148(7):2207-2216.
16. Tait JF, Smith C. Phosphatidylserine receptors: role of CD36 in binding of anionic phospholipid vesicles to monocytic cells. *J Biol Chem.* 1999;274(5):3048-3054.
17. Henson PM, Bratton DL, Fadok VA. Apoptotic cell removal. *Curr Biol.* 2001;11(19):R795-805.
18. Oussoren C, Storm G. Liposomes to target the lymphatics by subcutaneous administration. *Adv Drug Deliv Rev.* 2001;50(1-2):143-156.
19. Lindh I, Stawinski J. A general method for the synthesis of glycerophospholipids and their analogs via H-phosphonate intermediates. *J Org Chem.* 1989;54(6):1338-1342.

20. Ogihara-Umeda I, Sasaki T, Kojima S, Nishigori H. Optimal radiolabeled liposomes for tumor imaging. *J Nucl Med.* 1996;37(2):326-332.
21. Mauldin JP, Srinivasan S, Mulya A, et al. Reduction in ABCG1 in Type 2 diabetic mice increases macrophage foam cell formation. *J Biol Chem.* 2006;281(30):21216-21224.
22. Lowry OH, Rosebrough NJ, Farr AL, Randall RJ. Protein measurement with the Folin phenol reagent. *J Biol Chem.* 1951;193(1):265-275.
23. Tsukada T, Rosenfeld M, Ross R, Gown AM. Immunocytochemical analysis of cellular components in atherosclerotic lesions. Use of monoclonal antibodies with the Watanabe and fat-fed rabbit. *Arteriosclerosis.* 1986;6(6):601-613.
24. Ogawa M, Nakamura S, Saito Y, Kosugi M, Magata Y. What can be seen by 18F-FDG PET in atherosclerosis imaging? The effect of foam cell formation on 18F-FDG uptake to macrophages in vitro. *J Nucl Med.* 2012;53(1):55-58.
25. Milla P, Dosio F, Cattel L. PEGylation of proteins and liposomes: a powerful and flexible strategy to improve the drug delivery. *Curr Drug Metab.* 2012;13(1):105-119.
26. Almer G, Wernig K, Saba-Lepek M, et al. Adiponectin-coated nanoparticles for enhanced imaging of atherosclerotic plaques. *Int J Nanomedicine.* 2011;6:1279-1290.
27. Li D, Patel AR, Klibanov AL, et al. Molecular imaging of atherosclerotic plaques targeted to oxidized LDL receptor LOX-1 by SPECT/CT and magnetic resonance. *Circ Cardiovasc Imaging.* 2010;3(4):464-472.
28. Mulder WJ, Douma K, Koning GA, et al. Liposome-enhanced MRI of neointimal lesions in the ApoE-KO mouse. *Magn Reson Med.* 2006;55(5):1170-1174.
29. Torchilin VP. Recent advances with liposomes as pharmaceutical carriers. *Nat Rev Drug Discov.* 2005;4(2):145-160.

Table 1 Biodistribution of [^{111}In]PS100 in normal mice.

	Time after injection (min)					
Organ	1	5	20	60	120	240
Blood	18.4 ± 2.38	1.54 ± 0.31	0.98 ± 0.09	1.01 ± 0.22	0.74 ± 0.15	0.66 ± 0.06
Intestine	0.29 ± 0.06	0.19 ± 0.03	0.23 ± 0.08	0.26 ± 0.05	0.23 ± 0.07	0.42 ± 0.01
Kidney	2.33 ± 0.32	2.84 ± 0.36	3.33 ± 0.49	3.24 ± 0.59	3.49 ± 0.28	4.00 ± 0.29
Liver	34.9 ± 2.60	58.9 ± 6.50	62.6 ± 8.10	62.1 ± 4.16	57.8 ± 8.75	59.3 ± 3.03
Stomach	0.27 ± 0.08	0.53 ± 0.28	0.21 ± 0.06	0.29 ± 0.10	0.31 ± 0.15	0.41 ± 0.17
Spleen	14.3 ± 4.42	42.4 ± 11.4	36.7 ± 7.40	40.9 ± 7.32	42.3 ± 10.9	44.5 ± 4.71
Pancreas	0.50 ± 0.07	0.36 ± 0.01	0.30 ± 0.06	0.48 ± 0.27	0.30 ± 0.06	0.30 ± 0.07
Lung	9.51 ± 3.81	1.49 ± 0.16	0.99 ± 0.10	1.17 ± 0.57	0.72 ± 0.08	0.76 ± 0.12
Heart	2.50 ± 0.64	0.61 ± 0.13	0.46 ± 0.06	0.49 ± 0.09	0.42 ± 0.07	0.44 ± 0.04

*Each value represents mean ± S.D. (%dose/g, n=4 or 5).

Table 2 Biodistribution of [^{111}In]PS200 in normal mice.

	Time after injection (min)					
Organ	1	5	20	60	120	240
Blood	13.1 ± 5.88	3.16 ± 0.55	3.29 ± 0.57	2.92 ± 0.36	2.44 ± 0.50	1.95 ± 0.53
Intestine	0.48 ± 0.12	0.46 ± 0.08	0.44 ± 0.09	0.61 ± 0.16	0.68 ± 0.24	0.86 ± 0.26
Kidney	3.89 ± 1.05	8.98 ± 1.53	9.23 ± 1.96	8.95 ± 1.31	11.0 ± 3.48	12.0 ± 3.07
Liver	22.3 ± 5.96	32.8 ± 5.01	35.2 ± 3.47	36.0 ± 3.30	37.1 ± 6.12	39.1 ± 2.00
Stomach	0.41 ± 0.14	0.38 ± 0.11	0.45 ± 0.06	0.46 ± 0.13	0.39 ± 0.09	0.57 ± 0.22
Spleen	6.05 ± 2.09	20.7 ± 5.73	17.8 ± 5.38	19.0 ± 5.89	21.2 ± 2.96	23.8 ± 5.35
Pancreas	1.05 ± 0.10	0.83 ± 0.14	0.70 ± 0.08	0.83 ± 0.04	0.66 ± 0.11	0.76 ± 0.09
Lung	9.93 ± 2.53	2.59 ± 0.47	2.37 ± 0.35	2.22 ± 0.39	2.14 ± 0.49	1.60 ± 0.36
Heart	2.44± 0.79	1.09 ± 0.17	1.01 ± 0.16	1.11 ± 0.22	0.93 ± 0.15	0.91 ± 0.25

*Each value represents mean ± S.D. (%dose/g, n=4 or 5).

Table 3 Biodistribution of [^{111}In]PC100 in normal mice.

	Time after injection (min)					
Organ	1	5	20	60	120	240
Blood	32.9 ± 4.08	30.1 ± 0.46	17.0 ± 5.99	5.75 ± 4.63	0.52 ± 0.49	1.58 ± 1.96
Intestine	0.40 ± 0.05	0.46 ± 0.06	0.37 ± 0.16	0.28 ± 0.13	0.23 ± 0.10	0.59 ± 0.33
Kidney	3.43 ± 0.50	3.51 ± 0.17	3.02 ± 0.96	2.28 ± 0.99	1.56 ± 0.38	3.39 ± 1.63
Liver	6.34 ± 1.67	12.5 ± 2.66	28.1 ± 6.65	47.2 ± 5.75	53.8 ± 6.85	46.5 ± 13.4
Stomach	0.45 ± 0.14	0.56 ± 0.23	0.43 ± 0.14	0.40 ± 0.16	0.39 ± 0.21	0.44 ± 0.14
Spleen	5.16 ± 2.77	17.9 ± 3.20	101 ± 32.6	171 ± 69.4	174 ± 68.3	193 ± 53.7
Pancreas	0.65 ± 0.14	0.66 ± 0.09	0.54 ± 0.25	0.32 ± 0.21	0.21 ± 0.19	0.84 ± 0.48
Lung	18.9 ± 7.76	11.8 ± 1.51	6.62 ± 1.91	3.48 ± 2.55	0.64 ± 0.50	2.66 ± 2.20
Heart	4.33 ± 0.88	3.31 ± 1.00	2.08 ± 0.76	0.78 ± 0.63	0.19 ± 0.07	0.53 ± 0.54

*Each value represents mean ± S.D. (%dose/g, n=4 or 5).

Table 4 Biodistribution of [^{111}In]PC200 in normal mice.

	Time after injection (min)					
Organ	1	5	20	60	120	240
Blood	33.2 ± 4.03	18.6 ± 5.01	6.83 ± 3.47	2.57 ± 1.33	1.10 ± 0.13	0.65 ± 0.10
Intestine	0.36 ± 0.07	0.31 ± 0.05	0.27 ± 0.03	0.28 ± 0.07	0.32 ± 0.14	0.32 ± 0.09
Kidney	3.35 ± 0.62	3.38 ± 0.51	4.81 ± 1.03	4.38 ± 0.75	4.72 ± 0.67	5.41 ± 1.02
Liver	8.08 ± 2.32	26.7 ± 8.32	38.6 ± 4.17	48.8 ± 3.38	49.4 ± 6.14	46.2 ± 7.84
Stomach	0.54 ± 0.22	0.44 ± 0.16	0.44 ± 0.13	0.40 ± 0.14	0.33 ± 0.20	0.28 ± 0.11
Spleen	10.0 ± 4.24	49.4 ± 12.2	72.2 ± 15.5	112 ± 30.3	142 ± 43.8	173 ± 76.2
Pancreas	0.71 ± 0.27	0.58 ± 0.18	0.44 ± 0.14	0.43 ± 0.10	0.45 ± 0.15	0.38 ± 0.15
Lung	20.8 ± 3.74	9.89 ± 1.79	4.20 ± 1.95	2.00 ± 0.74	1.62 ± 1.02	0.99 ± 0.24
Heart	6.05 ± 2.53	2.95 ± 1.71	1.02 ± 0.39	0.56 ± 0.22	0.49 ± 0.13	0.33 ± 0.07

*Each value represents mean ± S.D. (%dose/g, n=4 or 5).

FIGURE LEGENDS

FIGURE 1.

^{111}In-labeled liposome uptake by cultured macrophages. A significantly higher uptake was observed in PS liposomes compared to PC liposomes of each size (*P<0.05). D isomer of PS liposomes showed lower uptake than L isomers.

Fig. 1

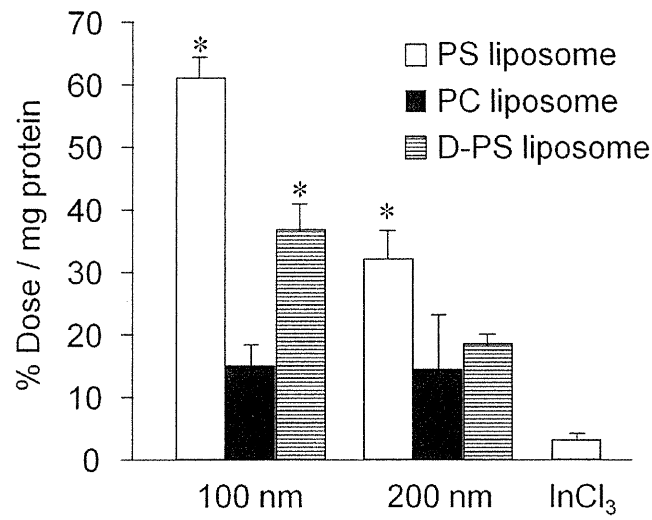

FIGURE 2.

En face autoradiography of ApoE -/- mice aorta. Photographic images of unstained aorta (A), images after Oil Red O staining (B), autoradiograms (C), and target-to-nontarget ratio (TNR) (D). The autoradiograms were well matched with Oil Red O staining. TNR was significantly higher in PS liposomes than PC liposomes in each size (*P<0.05). PS200 showed higher TNR than PS100 (†P<0.05).

Fig. 2

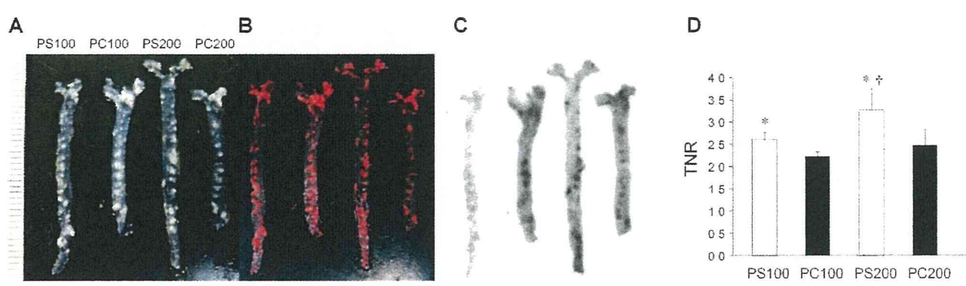

FIGURE 3.

SPECT and CT images, *ex vivo* ARG, and histological images of [^{111}In]PS100 (A) and [^{111}In]PS200 (B) in WHHL rabbits, and [^{111}In]PS200 in a normal rabbit (C). The white arrows indicate the position of the aorta. "L" represents the liver. Magnified images of Azan-Mallory staining show a macrophage foam cell-rich region with less smooth muscle cells (dashed red circle), and a more fibrotic region with dead macrophages (dashed yellow circle). The atherosclerotic regions were successfully visualized with [^{111}In]PS200 and [^{111}In]PS100 in WHHL rabbits. The radioactivity was accumulated in macrophage foam cell area, and was low in the fibrotic area. No aortic accumulation was seen in a normal rabbit.

Fig. 3